Journal of The Electrochemical Society

Zinc-Iron Flow Batteries with Common Electrolyte

To cite this article: S. Selverston *et al* 2017 *J. Electrochem. Soc.* **164** A1069

Zinc-Iron Flow Batteries with Common Electrolyte

S. Selverston,*,z R. F. Savinell, and J. S. Wainright*****

Department of Chemical and Biomolecular Engineering, Case Western Reserve University, Cleveland, Ohio 44106, USA

The feasibility of zinc-iron flow batteries using mixed metal ions in mildly acidic chloride electrolytes was investigated. Iron electrodeposition is strongly inhibited in the presence of Zn^{2+} and so the deposition and stripping processes at the negative electrode approximate those of normal zinc electrodes. In addition, the zinc ions have no significant effect on the Fe(II/III) couple at the positive electrode. This enables the use of mixed Zn-Fe electrolytes and microporous separators in place of expensive ion-exchange membranes. Considering the low-cost materials and simple design, zinc-iron chloride flow batteries represent a promising new approach in grid-scale energy storage. The preferential deposition of zinc occurs with similar behavior on titanium, graphite and glassy carbon substrates. A proof-of-concept zinc-iron chloride battery starting with mixed electrolytes was demonstrated and maintains a consistent open-circuit voltage of about 1.5 V and stable performance during over 10 days and 100 cycles of continuous charge-discharge cycling.

Manuscript submitted December 7, 2016; revised manuscript received February 23, 2017. Published March 22, 2017.

Zinc-based hybrid flow batteries are being widely-developed due to the desirable electrochemical properties of zinc such as its fast kinetics, negative potential ($E^0 = -0.76$ V_{SHE}) and high overpotential for the hydrogen evolution reaction (HER). Many groups are developing zinc-bromine batteries, and they address challenges associated with bromine toxicity and the organic complexing agents used to reduce its vapor pressure.[1,2] Other positive electrode couples using cerium, vanadium, nickel and iron are also being investigated.[3–5] Zinc-ferricyanide flow batteries using alkaline electrolytes were developed in the late 1970 s, but progress was reportedly hindered by high membrane costs and challenges with handling solid zinc oxide precipitates.[6] Currently, zinc-ferricyanide flow batteries are also being developed by ViZn, Inc.[7] Some of the challenges of using the $Fe(CN)_6^{3-/4-}$ couple include its low solubility on the order of 0.2–0.5 mol L^{-1}, and the possible generation of toxic gas if it mixes with acid.[8–10] More recently, a zinc-iron flow battery based on deep eutectic solvents (DES) with an open-circuit potential of 1.02 V was described, but it operated at a low current density of 0.5 mA cm^{-2} and so it was concluded that high-temperature operation would be required in order to obtain useful power densities.[11]

Of the possible reactions to use for a positive electrode, the aqueous Fe(II/III) redox couple is among the safest and cheapest, and it has high solubility and fast kinetics even on uncatalyzed carbon materials.[12] However, most studies of zinc-iron batteries have focused on the alkaline chemistry (using $Fe(CN)_6^{3-/4-}$ at the positive electrode), and there are only a few reports of zinc-iron flow batteries based on the acidic chemistry. A recent study combined an alkaline (2.4 M NaOH) negative electrode with an acidic (1 M HCl) positive electrode to achieve high performance, but this required the use of two ion-exchange membranes as well as a third electrolyte pump.[13] In 2016, an acidic zinc-iron sulfate battery employing an ion-exchange membrane demonstrated 50 charge-discharge cycles at 30 mA cm^{-2} from a bath containing 1.5 mol L^{-1} H_2SO_4 and acetate buffers.[14] During battery cycling, the authors observed a performance fade and attributed it to crossover of iron ions. Therefore, it was stated that it would not be possible to operate a battery with a mixed zinc-iron electrolytes because any Fe^{2+} or Fe^{3+} present in the negative electrolyte would be reduced in place of the zinc ions, and it was concluded that future work should focus on development of more selective membranes.

In conventional (single-membrane) architectures, the ion-exchange membranes ($120-500 m^{-2}), can account for 20–40 % of the flow battery cost, and their use has been called "the stumbling block" toward flow battery commercialization.[15,16] Whereas previous studies have used such membranes to prevent electrolyte mixing, this work investigates battery operation using mixed electrolytes in order to simplify the battery hardware and to reduce capital costs. As with the all-iron flow battery, moderate amounts of electrolyte crossover in this configuration would not cause irreversible performance loss.[17] Furthermore, the battery could operate using microporous separators (normally based on polyethylene or polypropylene), which are less expensive than ion-exchange membranes by more than an order of magnitude.[18] It should also be noted that in lightly-acidic iron chloride solutions, the conductivity of proton exchange membranes can be much lower than in more acidic solutions due to their conversion to an iron form rather than the desired proton form.

It might be expected that an electrodeposit made from the mixed $ZnCl_2$-$FeCl_2$ electrolytes would be an alloy of the two metals, and that the incorporation of iron would significantly decrease both the voltaic efficiency and the coulombic efficiency; the reduction in voltaic efficiency would be expected because of the more positive potential of iron ($E^0 = -0.44$ V vs SHE) compared to zinc ($E^0 = -0.76$ V vs SHE), and the reduction in coulombic efficiency could be expected since iron is a relatively good catalyst for hydrogen evolution.[19] However, anomalous codeposition (ACD) phenomena allow for preferential zinc plating from electrolytes containing zinc mixed with iron-group metal ions.[20–23] This study shows that it's possible to use the ACD to enable a pseudo-zinc negative electrode that operates from mixed $ZnCl_2$-$FeCl_2$ electrolytes, as illustrated in Figure 1. The associated reactions for the negative electrode, positive electrode and overall cell reaction of such a system are given by Equations 1, 2 and 3, respectively.

$$Zn^{2+} + 2e^- \underset{dis}{\overset{chg}{\rightleftharpoons}} Zn \qquad E^0 = -0.76 \text{ V} \qquad [1]$$

$$Fe^{3+} + e^- \underset{chg}{\overset{dis}{\rightleftharpoons}} Fe^{2+} \qquad E^0 = +0.77 \text{ V} \qquad [2]$$

$$Zn^{2+} + 2Fe^{2+} \underset{dis}{\overset{chg}{\rightleftharpoons}} Zn + 2Fe^{3+} \qquad E^0 = 1.53 \text{ V} \qquad [3]$$

The anomalous behavior of electroplating from such mixed electrolytes has been attributed to the so-called hydroxide suppression mechanism (HSM), wherein the formation of a surface hydroxide layer (e.g., $Zn(OH)_2$) impedes the transport of the more noble

*Electrochemical Society Student Member.
**Electrochemical Society Fellow.
***Electrochemical Society Member.
zE-mail: ss@case.edu

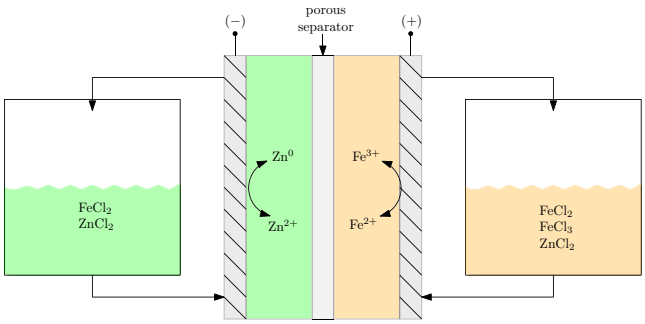

Figure 1. Schematic of a zinc-iron chloride flow battery with mixed electrolytes.

metal ions to the underlying substrate.[24,25] However, other reports concluded that the HSM was inconsistent with experimental data, and there is still no universally-accepted mechanism for anomalous codeposition.[20,26–29] Although more research is needed to fully understand ACD, in this study we take advantage of the ACD phenomena for application in a flow battery.

Electrodeposition from related mixed electrolytes has been studied for alloy plating applications, where there are different requirements and performance metrics than there are for battery applications. In alloy deposition, for example, it is desired to incorporate iron into the deposit because the alloy has superior corrosion resistance compared to pure zinc.[30–34] However, the coulombic efficiency during plating decreases with increasing iron incorporation into the alloy.[31] For zinc-iron battery applications, it would be ideal to completely inhibit iron deposition in order to maintain the zinc potential and hinder hydrogen evolution. Furthermore, for battery applications, there can be additional challenges due to the galvanic displacement during discharge via Equation 4. If the galvanic displacement of zinc by iron is slow, then the charge-discharge processes can be carried out with performance similar to that which could be obtained from a "pure" electrolyte containing only Zn^{2+} as the active metal cation in the negative electrolyte. This study investigated the plating and stripping processes of zinc, iron and their mixtures at pH=1 in order to avoid the formation of insoluble iron hydroxide precipitates, which can form between 2<pH<3 and possibly interfere with the measurements, while minimizing hydrogen evolution.[12,17,35]

$$Zn + Fe^{2+} \rightarrow Fe + Zn^{2+} \qquad E^0 = 0.32\ V \qquad [4]$$

Methods

Using an H-Cell with a Luggin capillary, deposition and dissolution were examined using solutions containing iron chloride, zinc chloride, and their mixtures. The solution pH was adjusted by dropwise addition of 10 $\%_w$ HCl. Titanium bar (0.020", grade 2A, ASTM B265, $A = 1\ cm^2$) and glassy carbon ($A = 0.197\ cm^2$) were used as substrates. Initial pre-treatment of the titanium consisted of washing in detergent with hot water followed by rinsing in acetone and isopropyl alcohol. Subsequently, the electrode was sanded by hand (120-grit, Norton T461) to remove surface oxides. Unless otherwise noted, 1 mol L^{-1} NH_4Cl was used as a supporting electrolyte. Cyclic voltammetry was carried out by scanning the potential from −0.2 to −1.3 V vs AgCl at scan rates, ν, ranging from 2–50 mV s^{-1} using a Solartron Modulab potentiostat. Effects of transport were studied using a rotator (Pine, Inc.) with a glassy carbon electrode ($A = 0.197\ cm^2$). A flow battery ($A = 6.25\ cm^2$) consisting of graphite plates as electrodes and a microporous separator (Daramic 175, thickness = 175 μm) was used, with the flow provided by peristaltic pumps at 50 mL min^{-1}. The positive electrode employed 2-mm thick carbon felt bonded to the graphite plate, as described elsewhere.[35] Teflon gaskets (2-mm thick) were used on each side of the separator. The electrolytes were prepared to simulate operation at 30 % SoC, assuming a starting composition of 1.6 M $ZnCl_2$ and 0.8 M $FeCl_2$ in both compartments. Therefore, the initial negative electrolyte contained 1.12 mol L^{-1} $ZnCl_2$ and 0.8 mol L^{-1} $FeCl_2$, and the initial positive electrolyte contained 1.6 mol L^{-1} $ZnCl_2$, 0.56 mol L^{-1} $FeCl_2$ and 0.24 mol L^{-1} $FeCl_3$. Both electrolytes contained 2 mol L^{-1} NH_4Cl supporting electrolyte and 2 g L^{-1} PEG_{8000} to moderate dendrite growth,[36] and the volume of each electrolyte was 175 mL. Charging and discharging were carried out at ± 25 mA cm^{-2}. Coulombic and voltaic efficiencies were estimated using $CE = q_{discharge}/q_{charge}$ and $VE = \bar{E}_{discharge}/\bar{E}_{charge}$, where q represents charge in coulombs and $\bar{E}$ represents the average value of potential. Battery charging was carried out for one hour, and discharges were carried out until the cell reached a cutoff voltage of 0 V to completely strip any deposited metal. This represented a SoC swing of about 1.5 % based on the Zn^{2+} in the negative electrolyte and 4.2 % based on the Fe^{2+} in the positive electrolyte. Temperature was maintained at 25 °C using an in-line shell-and-tube heat exchanger.

Results and Discussion

The chloride medium was chosen for this study because electrolytes containing chloride tend to promote greater current efficiency (lower H_2 evolution rates) and conductivity than those containing sulfate.[31,37–39] A comparison between the voltammograms of the iron, zinc, and mixed zinc-iron systems is shown in Figure 2. It is noteworthy that in the iron-only solution ($E^0 = -0.66\ V_{Ag/AgCl}$), there is about 360 mV of overpotential before the onset of significant reduction currents, compared to about 80 mV for zinc-containing solutions ($E^0 = -0.98\ V_{Ag/AgCl}$). Due to the high overpotential for iron deposition, the reduction curves for iron and zinc occur within about 50 mV of one another despite a 300 mV difference in their standard reduction potentials.

As can be observed in Figure 2a, reduction currents for the iron-only electrolyte started at approximately −1.0 V versus Ag/AgCl, and the stripping current occurred in the region of −0.6 to −0.2 V. When the equimolar zinc-iron solution was used, however, there was no significant iron stripping peak despite a clear zinc stripping peak in the region of −1.0 to −0.8 V. Based on the polarization curves, normal alloy plating theory would expect that iron reduction should have also taken place concurrently, but this was not observed. After plating at low overpotentials (less-negative scan limits), iron stripping peaks were not observed, even when zinc plating and stripping took place. When scanning the potential to more negative limits, however, subsequent iron stripping peaks were present, as shown in Figure 2b. While the iron stripping peaks were nearly absent when scanning to −1100 mV, −1150 mV and −1200 mV, the scans at −1250 mV and −1300 mV displayed noticeable iron stripping peaks at ca. −0.6 V. These results were consistent with a previous study, which also reported increasing iron content with more negative scan limits in NaCl solution with Zn/Fe = 1/3.[39]

Since iron stripping peaks were observed under some conditions, which would be undesirable for a flow battery, further experiments were conducted in order to compare the effects of pH, Zn/Fe molar ratio and zinc transport on the deposition and stripping behavior. First, voltammograms were carried out from quiescent solution onto titanium substrate at pH = 1 and pH = 3 at three different Zn/Fe molar ratios. As shown in Figure 3, it was found that iron stripping peak currents increased at lower Zn/Fe molar ratios, but there was little difference between voltammograms from the pH = 1 and pH = 3 solutions. In addition to the formation of the iron stripping peak, more negative scan limits were also associated with the bifurcation of the peak in the zinc region into two separate peaks. This behavior has been attributed to the formation of a Zn+Fe solid solution η-phase, wherein the first peak corresponds to the zinc in the η-phase, the second corresponds to the iron in the η-phase, and peak in the iron-stripping region (−0.45 to −0.6 V vs Ag/AgCl) corresponds to pure α-phase iron.[39] In order to further elucidate the roles of Zn/Fe molar ratios and zinc ion transport, additional experiments were carried out using a rotating disk electrode with a glassy carbon substrate.

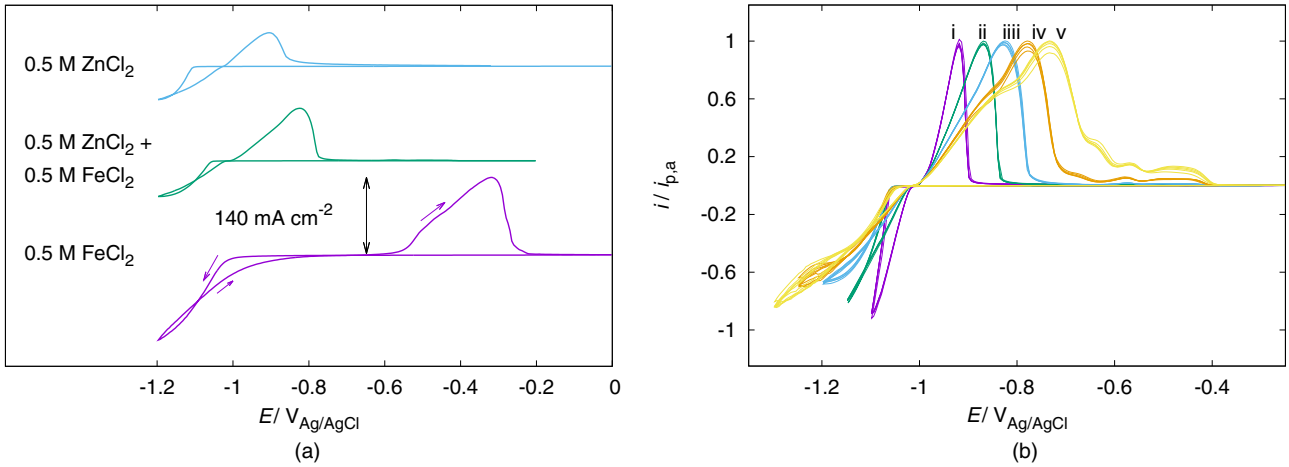

Figure 2. (a) Deposition and dissolution at pH=1 and $\nu = 10$ mV s^{-1} when scanning to −1.2 V versus Ag/AgCl from zinc and iron chloride electrolytes onto titanium substrate in quiescent solution, and (b) effect of negative scan limit ($\nu = 10$ mV s^{-1}) on deposition and stripping from equimolar $ZnCl_2$-$FeCl_2$ solutions, where current is normalized to the peak stripping current; (i) is −1100 mV, (ii) is −1150 mV, (iii) is −1200 mV, (iv) is −1250 mV, and (v) is −1300 mV. All solutions contained NH_4Cl supporting electrolyte adjusted to maintain 3 mol L^{-1} Cl^-.

As shown in Figure 4a, reduction currents between 20–30 mA cm^{-2} were measured at rotation rates of 300< ω <1500 rpm without any observable iron stripping peaks from an equimolar $ZnCl_2$-$FeCl_2$ solution with negative scan limit of −1150 mV vs Ag/AgCl. That is, the zinc appeared to be deposited preferentially via an ACD mechanism. Since zinc-based flow batteries often charge at 10–50 mA cm^{-2},[2] this result suggested that zinc-rich deposits can be made (viz., the ACD process can be utilized) from mixed electrolytes at useful current densities in flow battery applications. Although not presented, XPS analysis was also used to confirm the predominance of zinc in the deposit surfaces. In order to obtain more insight into the deposition and stripping, further tests were conducted at more negative scan limits (higher plating current densities), as shown Figures 4b, 4c and 4d. Here, some iron stripping peaks were observed, particularly at the lowest rotation rate (ω = 300 rpm). Similar to the other experiments from quiescent solution at low Zn/Fe molar ratios (Figure 3), the zinc stripping peak bifurcated into two separate peaks when plating at higher current densities. When the rotation rate was increased though, the associated stripping current went from showing three peaks (two in the zinc region and one in the iron region) to showing only one peak. That is, faster rotation rates were necessary in order to keep up with higher current densities while avoiding bifurcation of the zinc stripping peak as well as formation of iron stripping peaks. The behavior from the mixed solution was also compared with a zinc-only control solution, as shown in Figure 5 for a negative scan limit of −1350 mV vs Ag/AgCl. It is clear that at relatively higher plating current densities ($i > 50$ mA cm^{-2}), faster rotation rates led to stripping peaks that looked closer to the those from the zinc-only solution.

These results seemed to disagree with the HSM theory, whereby the anomalous behavior should be enhanced by increasing pH (or equivalently, by decreasing the electrode rotation rate so that a significant pH gradient can be established). In Figure 4a, for example, there were clear zinc stripping peaks present but no iron stripping peaks, despite plating on a disk spinning at 1500 rpm from a solution with an acidic solution (pH=1). It has been reported that the critical pH for zinc hydroxide precipitation is approximately pH = 5.18.[26,40] However, it can be shown that such a high surface pH is unlikely to exist on an electrode rotating at 1500 rpm, wherein the surface pH should be close to the bulk pH. Furthermore, HSM theory would predict a trend of decreasing anomalous behavior with increasing rotation rate (since increasing rotation rate is associated with a small pH gradient near the electrode surface), but the opposite trend was observed. This is consistent with several previous studies, which have noted similar discrepancies.[27,30] In the present results, the anomalous deposition

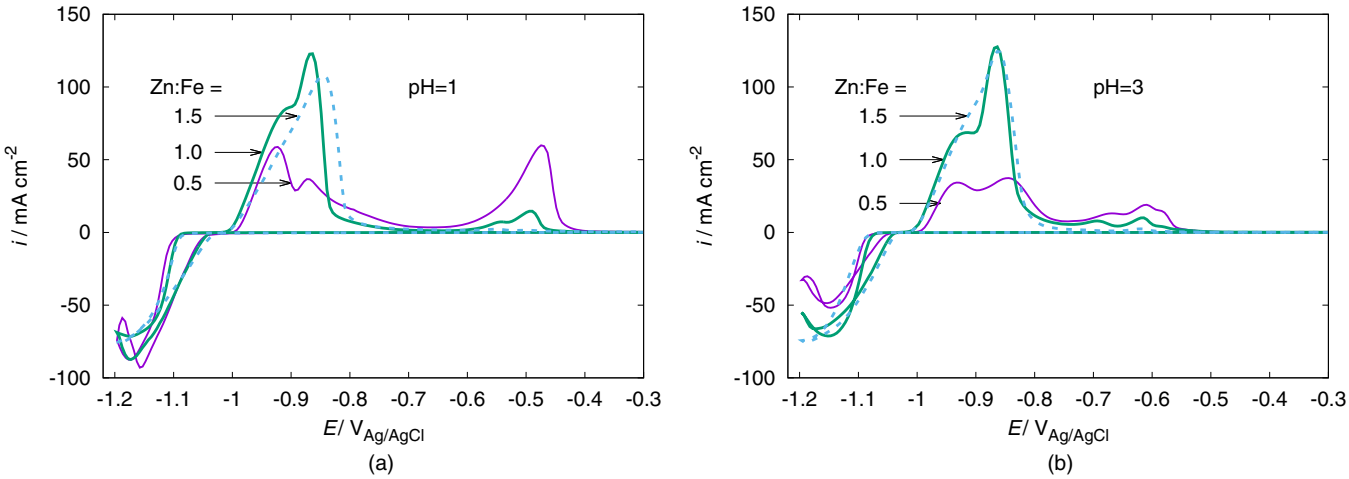

Figure 3. (a) Deposition and dissolution onto titanium substrate from quiescent solution for three Zn/Fe ratios at (a) pH=1 and (b) pH=3, where all solutions contained $C_{Me^{2+}} = 1$ mol L^{-1} and 3 mol L^{-1} NH_4Cl supporting electrolyte.

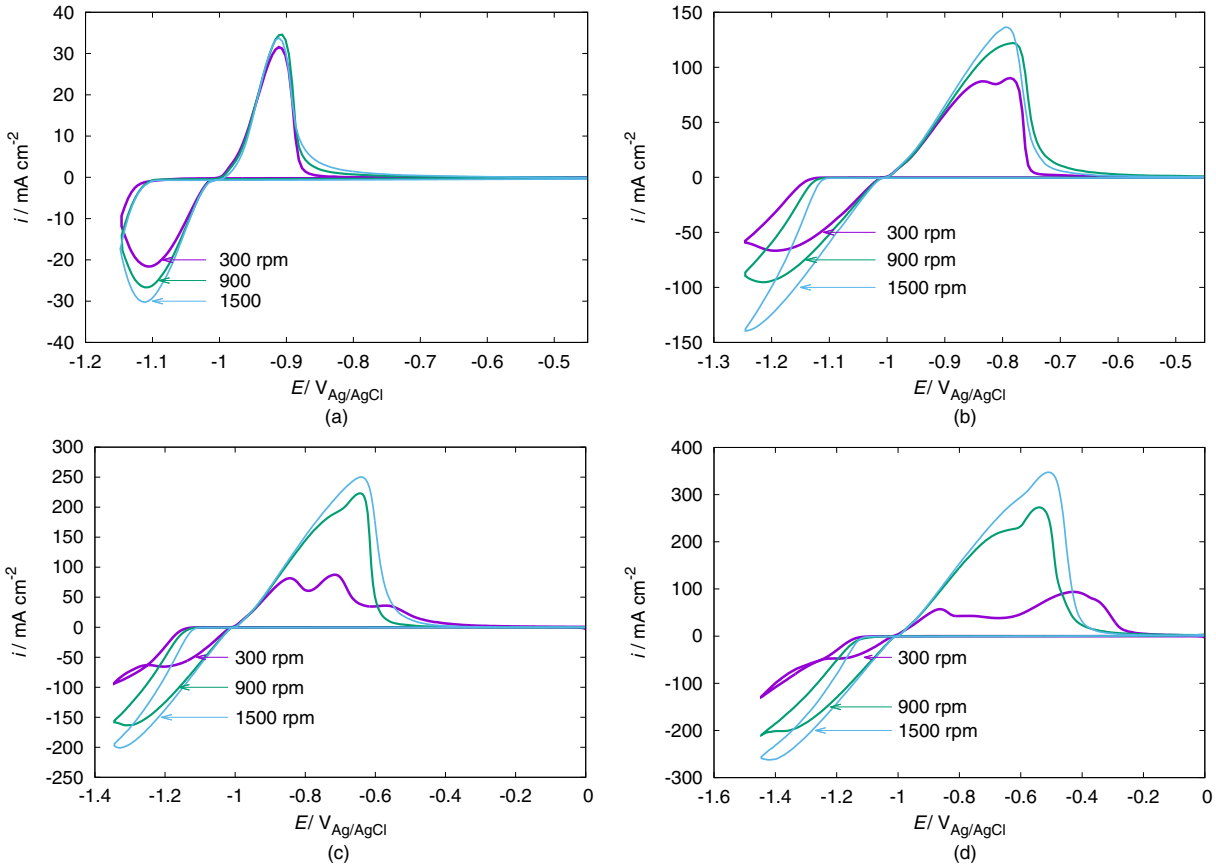

Figure 4. Effect of rotation rate and negative scan limit on deposition and stripping from electrolytes containing 0.5 mol L^{-1} $ZnCl_2$ + 0.5 mol L^{-1} $FeCl_2$ on glassy carbon. The scan rate was $\nu = 50$ mV s^{-1} and the negative scan limits were (a) −1150 mV, (b) −1250 mV, (c) −1350 mV and (d) −1450 mV vs Ag/AgCl. The solution contained 1 mol L^{-1} NH_4Cl supporting electrolyte.

was found to be enhanced with increasing rotation rate, rather than being hindered, consistent with the findings by Gómez et al. for both Zn-Co and Zn-Fe electroplating, which suggested that the anomalous behavior depended mainly on zinc ion transport.[27,39]

In terms of the positive Fe(II)/Fe(III) electrode, only a slight depression of the electrode activity was apparent in a solution containing excess zinc (0.2 mol L^{-1} $FeCl_2$, 0.2 mol L^{-1} $FeCl_3$, 0.8 mol L^{-1} $ZnCl_2$), and there was no significant difference in peak shifting with increasing scan rate between the two solutions (see Figure 6). In both cases, the peak current varied linearly ($R^2 > 0.99$) with the square root of the scan rate, consistent with fast reactions controlled by mass transport. This result confirms that in the mixed system, the positive Fe(II/III) electrode can behave in the same way as it does in iron-chromium, iron-hydrogen, and all-iron batteries.

A proof-of-concept battery operating at ($T = 25$ °C) was tested over 10 days and 127 cycles of continuous charge-discharge cycling at ± 25 mA cm^{-2}, where each charge was carried out for one hour (charge loading = 25 mAh cm^{-2}, a similar value of metal loading

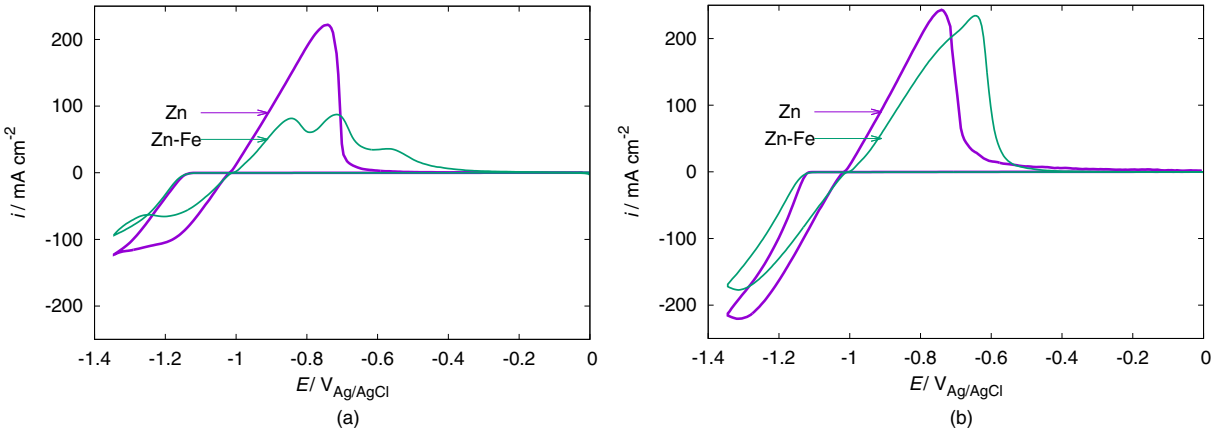

Figure 5. Comparison of deposition and stripping behavior between 0.5 mol L^{-1} $ZnCl_2$ and 0.5 mol L^{-1} $ZnCl_2$ + 0.5 mol L^{-1} $FeCl_2$ at (a) 300 rpm and (b) 1200 rpm on glassy carbon with $\nu = 50$ mV s^{-1} and negative scan limit of −1350 mV. The mixed solution contained 1 mol L^{-1} NH_4Cl and the zinc-only solution contained 2 mol L^{-1} NH_4Cl in order to maintain constant chloride concentration.

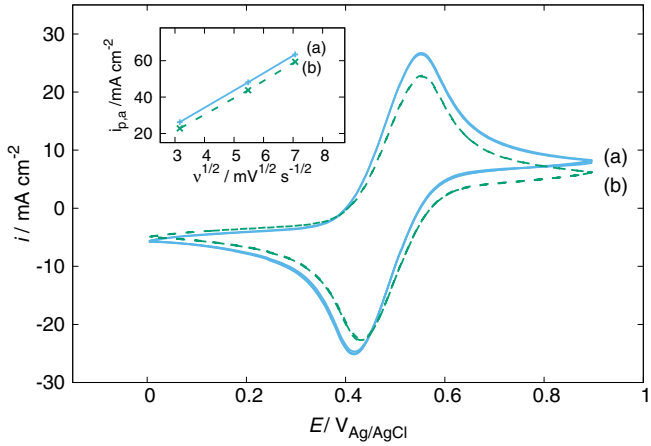

Figure 6. Effect of zinc chloride on Fe(II)/(III) redox reaction on graphite electrode with 1 mol L^{-1} NH_4Cl supporting electrolyte at pH=1 at $\nu = 10$ mV s^{-1}. Initial electrolyte (a) contained 0.2 mol L^{-1} Fe(II) and 0.2 mol L^{-1} Fe(III), and the modified electrolyte (b) also contained 0.8 mol L^{-1} Zn(II). Inset: scans performed at 10, 30, and 50 mV s^{-1} showed only a small decrease in the current peak.

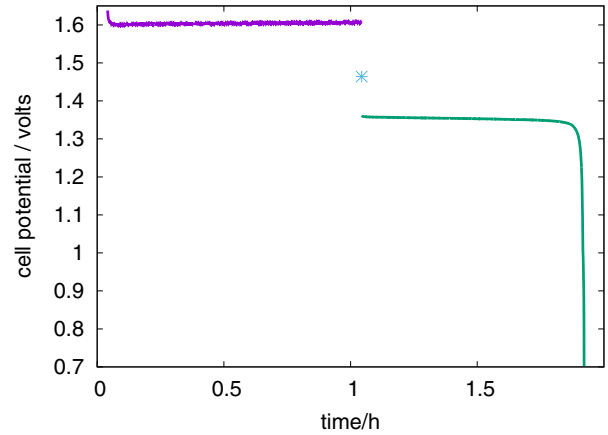

Figure 7. Close-up view of the first charge-discharge (Cycle # 1 in Figure 8) at ± 25 mA cm^{-2}, operating at $T = 25$ °C.

as described in Ref. 13). The open-circuit potential of about 1.5 V suggested that (1) the deposit contained primarily zinc, (2) the potential of the positive electrode was not affected by the presence of zinc and (3) the displacement of zinc by iron was not sufficiently fast so as to bring the electrode to the iron potential, where an OCV of about 1.2 V would have been observed. However, it was fast enough to produce some hydrogen gas as evidenced by visual inspection of the flowing electrolyte. Although this reaction does lead to some self-discharge, the electrolytes can be drained from the stacks during any gaps between charging and discharging in order to minimize any self-discharging when the battery is not in use. Voltage profiles were relatively flat, as shown for the first charge-discharge (Cycle # 1 of Figure 8) in Figure 7.

The cell potential of the battery during the first two days (25 cycles) is shown in Figure 8a, and the variation of efficiencies during 127 cycles over a 10-day period is shown in Figure 8b. The battery test was voluntarily stopped after 10 days, which was deemed to be sufficient for demonstrating operation of the mixed-electrolyte battery system. The performance was relatively stable, without any evidence of degradation. Initially, there was a pressure imbalance due to the fact that the positive electrolyte flowed through a porous felt whereas the negative electrolyte did not, so there was a gradual transfer of fluid from positive to negative. This was corrected by increasing the negative back-pressure with a needle valve (denoted as (i) in Figure 8b); this increased the stability and increased coulombic efficiency, presumably by decreasing the rate of crossover from the positive electrolyte. It was also noted that during cycles 20–50, voltaic efficiency decreased while coulombic efficiency increased (reaching a maximum of 95 %). Based on visual observation of the color of the flowing electrolyte, we speculate that this was due to the formation of some hydroxide precipitates, which formed a coating on the separator and hindered crossover of Fe^{3+} and protons from the positive electrolyte. During the 65th cycle, 2.5 g of citric acid (equivalent to about 35 mmol L^{-1}) was added to the electrolytes in order to complex the iron from the hydroxides (denoted as (ii) in Figure 8b); this caused an increase in voltaic efficiency and a corresponding decrease in coulombic efficiency. Both effects may be attributed to clearing of the separator pores. Based on these results, identification of the appropriate complexing ligands, as well as their optimum concentrations, is an important aspect of the development of zinc-iron chloride flow batteries. The average coulombic, voltaic and energy efficiencies were 85%, 80% and 68%, respectively, similar to those from Ref. 14, but operating with mixed electrolytes and a microporous separator. Considering the fast kinetics of the zinc and iron redox couples, the main source of low voltaic efficiency was likely the ohmic resistance in the separator and the large (∼2.2 mm) gap between positive and negative electrodes, as well as concentration polarization at the positive electrode (the Fe(II)/Fe(III) reaction is only a single-electron reaction, and the Fe^{2+} concentration was

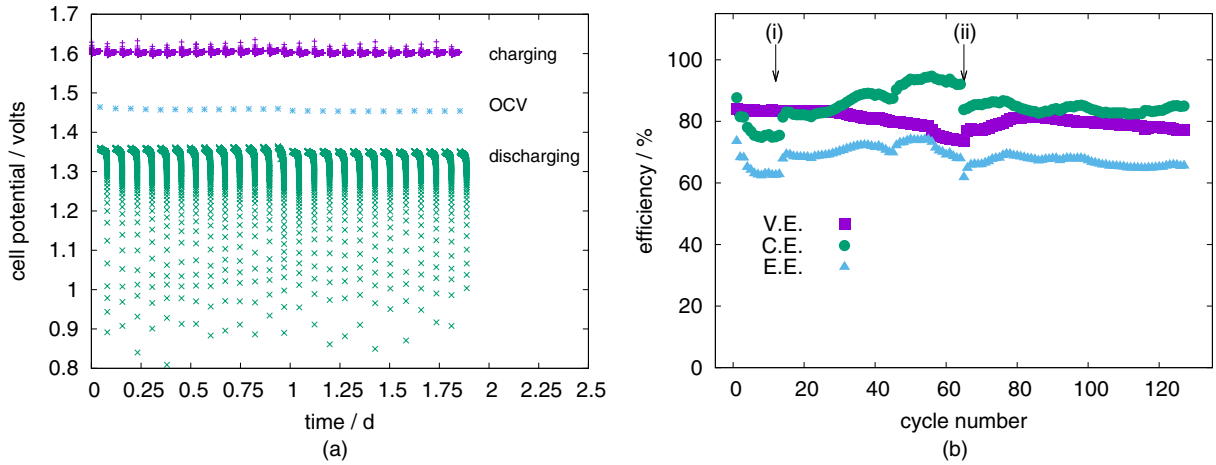

Figure 8. (a) Cell potential as a function of time during the first two days of testing, and (b) estimated voltaic, coulombic and energy efficiencies during over 10 days of continuous charge-discharge cycling at $T = 25$ °C.

relatively low). Cyclic voltammograms (not shown) indicated that the bulk plating and stripping processes were not significantly affected by the presence of the PEG. In the future, performance can be improved by optimizing various parameters such as the temperature, the electrolyte composition, the distance between electrodes, the electrode structure and the flow rate. It will also be important to determine the range of Zn:Fe and associated SoC that can be used for efficient battery operation; however, as with most hybrid flow batteries, any limitations on the amount of energy stored will be dictated primarily by the cell geometry and volume for zinc plating rather than by the SoC of the electrolyte. The coulombic efficiencies were lower than those in batteries using separated electrolytes and ion-selective membranes, but still high enough to obtain energy efficiencies of over 60% without optimization. It may be possible to reduce relative effects of both Fe^{3+} crossover as well as H_2 evolution by increasing the discharge current density, which would polarize the negative electrode in the positive direction. Also, in order to increase the stability for extended battery testing, an electrolyte rebalancing system should be incorporated in order to compensate for losing protons to hydrogen gas.[41] Most importantly, despite many days of operation using mixed electrolytes, neither the presence of Fe^{2+} nor Fe^{3+} in the negative electrolyte appeared to cause any irreversible performance degradation, and it was clear that zinc, rather than iron, was the primary species being deposited and stripped. The system cost was estimated using a model developed by PNNL,[42] modified as needed for the zinc-iron chloride architecture (e.g., $ZnCl_2$ and $FeCl_2$ electrolytes, Daramic separators, etc.). Assuming a discharge at 1.2 V and 50 mA cm^{-2}, we estimate the zinc-iron chloride battery system would cost about \$100 kWh^{-1} for a system capable of a 5.5 h discharge. However, achieving this will require additional research and development in order to better understand the cell behavior and the deposit morphology at higher states of charge.

Conclusions

It was shown that anomalous deposition of zinc from mixed $ZnCl_2$-$FeCl_2$ electrolytes can be used to enable zinc-iron chloride batteries that are crossover-tolerant and can use microporous separators. The inhibition of iron deposition by zinc ions was observed to occur without apparent dependence on substrate material, and iron incorporation into the deposits was only observed in cases with relatively low Zn/Fe (or high deposition current densities) that are outside the range of what is necessary for battery applications. The presence of excess zinc chloride (Zn/Fe = 4) only slightly depressed the activity of the Fe(II/III) reaction on graphite. A proof-of-concept flow battery demonstrated an OCV of approximately 1.5 V and good stability during continuous charge-discharge cycling at 25 °C. Based on the cell behavior, it was clear that the primary processes occurring at the negative electrode were zinc deposition and stripping, even when mixed with relatively high concentrations of Fe^{2+}. With further development, zinc-iron chloride batteries could achieve an excellent balance between cost, safety, and performance for grid-scale energy storage applications.

Acknowledgments

This work was sponsored by the Department of Energy, Office of Electricity under Sandia contract # 1111358,0. We would like to thank Nicholas Sinclair for the battery cost modeling work and Daramic, LLC for supplying membrane samples for the flow battery tests.

References

1. B. R. Chalamala, T. Soundappan, G. R. Fisher, M. R. Anstey, V. V. Viswanathan, and M. L. Perry, Redox flow batteries: An engineering perspective, *Proc. IEEE*, **102**, 1 (2014).
2. G. L. Soloveichik, Flow Batteries: Current Status and Trends, *Chem. Rev.*, **115**, 11533 (2015).
3. L. Zhang, J. Cheng, Y.-S. Yang, Y.-H. Wen, X.-D. Wang, and G.-P. Cao, Study of zinc electrodes for single flow zinc/nickel battery application, *J. Power Sources*, **179**, 381 (2008).
4. P. K. Leung, C. Leo, Ponce De León, and F. C. Walsh, An undivided zinc-cerium redox flow battery operating at room temperature (295 K), *Electrochem. Commun.*, **13**, 770 (2011).
5. P. K. Leung, C. Ponce De León, T. J. Low, and F. C. Walsh, Zinc deposition and dissolution in methanesulfonic acid onto a carbon composite electrode as the negative electrode reactions in a hybrid flow battery, *Electrochim. Acta*, **56**, 6536 (2011).
6. F. R. McLarnon and E. J. Cairns, The Secondary Alkaline Zinc Electrode, *J. Electrochem. Soc.*, **138**, 645 (1991).
7. S. Mullendore, What are flow batteries and how can they improve resiliency, continuity and safety in urban installations?, Resilient Power webinar (2016).
8. A. J. Esswein, J. Goeltz, and D. Amadeo, High solubility iron hexacyanides, *U. S. Patent App. US20140051003* **A1**, 1 (2014).
9. M. C. Tucker, V. Strinivasan, P. N. Ross, and A. Z. Weber, Performance and cycling of the iron-ion/hydrogen redox flow cell with various catholyte salts, *J. Appl. Electrochem.*, **43**, 637 (2013).
10. Safety Data Sheet for Potassium ferricyanide(III), www.sigmaaldrich.com.
11. D. Lloyd, T. Vainikka, M. Ronakainen, and K. Kontturi, Characterization and application of the Fe(II)/Fe(III) redox reaction in an ionic liquid analogue, *Electrochim. Acta* **109**, 843 (2013).
12. K. L. Hawthorne, J. S. Wainright, and R. F. Savinell, Studies of Iron-Ligand Complexes for an All-Iron Flow Battery Application, *J. Electrochem. Soc.*, **161**, A1662 (2014).
13. K. Gong, X. Ma, K. M. Conforti, K. J. Kuttler, J. B. Grunewald, K. L. Yeager, M. Z. Bazant, S. Gu, and Y. Yan, A zinc-iron redox-flow battery unter \$100 per kW h of system capital cost, *Energy Environ. Sci.*, **8**, 2941 (2015).
14. Z. Xie, Q. Su, A. Shi, B. Yang, B. Liu, J. Chen, X. Zhou, D. Cai, and L. Yang, High performance of zinc-ferrum redox flow battery with Ac/HAc buffer solution, *J. Energy Chem.*, **25**, 495 (2016).
15. H. Prifti, A. Parasuraman, S. Winardi, T. M. Lim, and M. Skyllas-Kazakos, Membranes for redox flow battery applications, *Membranes*, **2**, 275 (2012).
16. T. Janoschka, N. Martin, U. Martin, C. Friebe, S. Morgenstern, H. Hiller, M. D. Hager, and U. S. Schubert, An aqueous, polymer-based redox-flow battery using non-corrosive, safe, and low-cost materials, *Nature*, **527**, 78 (2015).
17. L. W. Hruska and R. F. Savinell, Investigation of Factors Affecting the Performance of the Iron Redox Battery, *J. Electrochem. Soc.*, **128**, 18 (1981).
18. J. A. Mellentine, Performance Characterization and Cost Assessment of an Iron Hybrid Flow Battery, M. S. Thesis, The School for Renewable Energy Science (2011).
19. J. McBreen, Rechargeable zinc batteries, *J. Electroanal. Chem.*, **168**, 415 (1984).
20. S. L. Díaz, O. R. Mattos, O. E. Barcia, and F. J. Fabri Miranda, ZnFe anomalous electrodeposition: stationary and local pH measurements, *Electrochim. Acta*, **47**, 4091 (2002).
21. R. Bhat, B. K. Udaya, and A. Chitharanjan Hegde, Optimization of deposition conditions for bright Zn-Fe coatings and its characterization, *Prot. Met. Phys. Chem. Surf.*, **47**, 645 (2011).
22. I. H. Karahan, Effects of pH value of the electrolyte and glycine additive on formation and properties of electrodeposited Zn-Fe coatings, *Sci. World J.*, **2013**, 1 (2013).
23. S. Amirat, R. Rehamnia, M. Bordes, and J. Creus, Zn-Fe alloy electrodeposition from chloride bath: Influence of deposition parameters on coatings morphology and structure, *Mater. Corros.*, **64**, 328 (2013).
24. H. Dahms and I. M. Croll, The Anomalous Codeposition of Iron-Nickel Alloys, *J. Electrochem. Soc.*, **112**, 771 (1965).
25. H. Fukushima, T. Akiyama, J.-h. Lee, M. Yamaguchi, and K. Higashi, Mechanism of the Electrodeposition of Zinc with Iron-Group Metals from Sulfate Baths, *Trans. Jpn. Inst. Met.*, **24**, 125 (1983).
26. X. Qiao, H. Li, W. Zhao, and D. Li, Effects of deposition temperature on electrodeposition of zinc-nickel alloy coatings, *Electrochim. Acta*, **89**, 771 (2013).
27. E. Chassaing and R. Wiart, Electrocrystallization mechanism of Zn-Ni alloys in chloride electrolytes, *Electrochim. Acta*, **37**, 545 (1991).
28. E. Gómez and E. Vallés, Electrodeposition of zinc cobalt alloys: inhibitory effect of zinc with convection and pH of solution, *J. Electroanal. Chem.*, **397** 177 (1995).
29. F. J. Fabri Miranda, O. E. Barcia, O. R. Mattos, and R. Wiart, Electrodeposition of Zn-Ni Alloys in Sulfate Electrolytes I. Experimental, *J. Electrochem. Soc.*, **144**, 3441 (1997).
30. G. Roventi, R. Cecchini, A. Fabrizi, and T. Bellezze, Electrodeposition of nickel zinc alloy coatings with high nickel content, *Surf. Coat. Technol.*, **276**, 1 (2015).
31. H. Fukushima, T. Akiyama, M. Yano, T. Ishikawa, and R. Kammel, Electrodeposition Behavior of Zn-Iron-group Metal Alloys from Sulfate and Chloride Baths, *ISIJ Int.*, **33**, 1009 (1993).
32. D. Crotty, Zinc alloy plating for the automotive industry, *Met. Finish.*, **94**, 54 (1996).
33. A. C. Hegde, K. Venkatakrishna, and N. Eliaz, Electrodeposition of Zn-Ni, Zn-Fe and Zn-Ni-Fe alloys, *Surf. Coat. Technol.*, **205**, 2031 (2010).
34. K. O. Nayana, T. V. Venkatesha, and K. G. Chandrappa, Influence of additive on nanocrystalline, bright Zn-Fe alloy electrodeposiiton and its properties, *Surf. Coat. Technol.*, **235**, 461 (2013).
35. K. L. Hawthorne, J. S. Wainright, and R. F. Savinell, Maximizing plating density and efficiency for a negative deposition reaction in a flow battery, *J. Power Sources*, **269**, 216 (2014).
36. S. Banik and R. Akolkar, Suppressing dendrite growth during zinc electrodeposition by PEG-200 additive., *J. Electrochem. Soc.*, **160**, D519 (2013).
37. G. D. Wilcox and D. R. Gabe, Electrodeposited zinc alloy coatings, *Corr. Sci.*, **35**, 1251 (1993).
38. R. Winand, Electrodeposition of Zinc and Zinc-Alloys, Modern Electroplating: Fifth Edition, 285 (2011).

39. E. Gómez, E. Pelaez, and E. Vallés, Electrodepostion of zinc + iron alloys: 1. Analysis of the initial stages of the anomalous codeposition, *J. Electroanal. Chem.*, **469**, 139 (1999).
40. K. Higashi, Mechanism of the electrodeposition of zinc alloys containing a small amount of cobalt, *J. Electrochem. Soc.*, **128**, 2081 (1981).
41. S. Selverston, R. F. Savinell, and J. S. Wainright, In-tank hydrogen-ferric ion recombination, *J. Power Sources*, **324**, 674 (2016).
42. V. Viswanathan, A. Crawford, D. Stephenson, S. Kim, W. Wang, B. Li, G. Coffey, E. Thomsen, G. Graff, P. Balducci, M. Kinter-Meyer, and V. Sprenkle, Cost and performance model for redox flow batteries, *J. Power Sources*, **247**, 1040 (2014).